

Constraining the $p\Lambda$ interaction from a combined analysis of scattering data and correlation functions

D. L. Mihaylov^{a,b,*}, J. Haidenbauer^{c,†} and V. Mantovani Sarti^{a,‡}

^a*Technische Universität München, Physics Department, James-Frank-Str., 85748 Garching, Germany*

^b*Sofia University, Faculty of Physics, 5 J. Bourchier Blvd, 1164 Sofia, Bulgaria and*

^c*Forschungszentrum Jülich, Institute for Advanced Simulation (IAS-4), 52428 Jülich, Germany*

This work provides the first combined analysis of low-energy $p\Lambda$ scattering, considering both cross section and correlation data. The obtained results establish the most stringent constraints to date on the two-body $p\Lambda$ interaction, pointing to a weaker attraction than so far accepted. The best set of scattering lengths for the spin singlet and triplet are found to range from $f_0, f_1 = (2.1, 1.56)$ to $(3.34, 1.18)$ fm. With a chiral NY potential fine-tuned to those scattering parameters, the in-medium properties of the Λ are explored and a potential depth of $U_\Lambda = -36.3 \pm 1.3(\text{stat})_{-6.2}^{+2.5}(\text{syst})$ MeV is found at nuclear matter saturation density.

Introduction: The strong interaction between nucleons (N) and hyperons ($Y=\Lambda, \Sigma, \Xi$) plays a significant role in various aspects of nuclear and hadronic physics, ranging from the structure and properties of hypernuclei to the Equation of State (EoS) of neutron stars (NS) [1, 2]. The recent observations of gravitational waves emitted from NS mergers [3, 4] and precise constraints on NS radii provided by the NICER collaboration [5–8] triggered a renewed interest in the presence of strange degrees of freedom in these compact objects [9, 10].

Specifically, the $N\Lambda$ system represents an important pillar for our understanding of the low-energy QCD dynamics between ordinary matter and strange particles [11]. Chiral effective field theory (χ EFT) [12–15] is an excellent tool to study the $N\Lambda$ interaction, since it offers the possibility to systematically improve the results by considering higher-order terms in the Lagrangian. These effective approaches rely on the availability of experimental data to determine the a priori unknown low-energy constants (LECs) associated with the contact interactions included in the Lagrangian. Until recently, the experimental constraints on the $N\Lambda$ interaction, and, in general, on the $S = -1$ baryon-baryon interaction, consisted primarily of scattering data [16–18] and measurements of Λ -hypernuclei binding energies [1, 19]. Elastic and inelastic cross section data, probing the transition $N\Lambda \leftrightarrow N\Sigma$, are relatively scarce and not available down to the threshold. Results from the COSY experiment delivered input on the $N\Lambda - N\Sigma$ dynamics by studying the $pp \rightarrow pK^+\Lambda$ [20, 21]. New scattering measurements on both $N\Lambda$ and $N\Sigma$ were reported by CLAS [22] and E40 [23–25] collaborations, adding constraints at higher momenta. Additionally, measured binding energies and lifetimes of light Λ -hypernuclei [1] provide complementary information on the strength of the $N\Lambda$ interaction, for example with regard to the hypertriton [26, 27] specifically on the singlet state [14].

Data on hypernuclei in the medium and heavy mass

regime have been employed to deduce the depth of the Λ single-particle potential U_Λ in infinite nuclear matter at nuclear saturation density $\rho_0 = 0.166 \text{ fm}^{-3}$. An overall attraction of ≈ -30 MeV is typically reported [1, 28], and this benchmark eventually serves as input for studies aiming to infer the behavior of Λ hyperons at NS core densities, reaching few times ρ_0 . Specifically, in investigations that commence with NY potentials describing $N\Lambda$ and $N\Sigma$ scattering data, the generally somewhat too attractive contribution from the two-body interaction is counterbalanced by an appropriate repulsive three-body NNA component to meet the ≈ -30 MeV constraint [29, 30].

In the last years, novel data based on two-particle correlations, involving strange hadrons, have become available and offer high-precision experimental insight into the $S = -1, -2, -3$ baryon-baryon interaction [31–37]. The recent measurement of the $p\Lambda$ correlation function in pp collisions at $\sqrt{s} = 13$ TeV by the ALICE Collaboration [32] provided the most precise data on this system down to threshold, accompanied by the first experimental observation of the opening of the coupled $N\Sigma$ channel in a two-body final state. Ongoing and future experimental efforts are posed to advance our understanding of the $N\Lambda$ interaction and the $N\Lambda \leftrightarrow N\Sigma$ dynamics. These efforts include the utilization of polarized Λ beams and high-precision hypernuclear spectroscopy [38], as well as statistically improved correlation functions during the ongoing LHC Run 3 data taking [39].

In this work, we, for the first time, perform a combined analysis of available $N\Lambda$ scattering and correlation data to constrain the corresponding $p\Lambda$ scattering parameters. The present study utilizes an Usmani-type potential and an interaction based on χ EFT. Anticipating our main finding, the analysis suggests an overall less attractive $N\Lambda$ interaction compared to what has formed the basis for theoretical investigations so far. To explore

the possible implications for the NS scenarios [29, 30], appropriately re-adjusted chiral potentials are employed to evaluate the single-particle potential U_Λ at ρ_0 .

p Λ interaction: For the analysis of the *p* Λ correlation data at low momenta, we employ wave functions generated from two different types of potentials. To thoroughly explore the sensitivity of the effective range parameters to the measured *p* Λ correlation functions, we use the Usmani potential [40], which includes spin dependence but lacks coupling to the $N\Sigma$ channel. This allows for a realistic description of the $N\Lambda$ interaction below the $N\Sigma$ threshold, which is relevant for determining the effective range parameters. The Usmani potential includes a Woods-Saxon-type repulsive core V_C , as well as a two-pion exchange tail constructed from a modified one-pion exchange tensor potential [41]. The repulsive core reads:

$$V_C(r) = W_C \left[1 + \exp\left(\frac{r - R_C}{d_C}\right) \right]^{-1}. \quad (1)$$

The parameters (W_C, R_C, d_C) are phenomenological in nature, and thus, we will adjust them in accordance with the analyzed data. The remaining parameters entering the Usmani potential are taken from [41].

In addition, we employ a modern NY potential derived within SU(3) χ EFT [13, 14], specifically, we utilize the NY potential NLO19 established in Ref. [14]. This potential incorporates contributions up to next-to-leading order (NLO) in the chiral expansion, in particular it includes contributions from one- and two-pseudoscalar-meson exchange diagrams, involving the Goldstone bosons π , K , η , and from four-baryon contact terms (without and with two derivatives), where the latter encode the unresolved short-distance dynamics. The LECs associated with these contact terms are free parameters and have been established by a global fit to a set of 36 *p* Λ and $N\Sigma$ low energy scattering data points [14], available since the 1960s. SU(3) flavor symmetry has been imposed which reduces the number of independent contact terms or LECs, respectively. Then, in the two *S*-wave states 1S_0 and 3S_0 , which dominate the scattering observables at low energies, there are 10 LECs [14], with two of them inferred from the NN sector via the imposed SU(3) symmetry.

The present work incorporates the *p* Λ correlation data measured by ALICE as an additional experimental constraint [42]. To accommodate this, some of the LECs have to be varied in the search for the optimal strength of the $N\Lambda$ interaction. Thereby, we aim at preserving the good description of the $p\Sigma^+$ and $p\Sigma^-$ data, as well as the $p\Sigma^- \rightarrow n\Lambda$ transition cross section provided by the original potential [14]. The simplest and most

efficient way to guarantee this is to relax the strict SU(3) symmetry for the contact interactions in the $N\Lambda$ and $N\Sigma$ forces [13, 14]. Therefore, following the procedure in [43], we introduce an SU(3) symmetry breaking in the leading-order contact terms that contribute to the $N\Lambda$ interaction in the relevant 1S_0 and 3S_1 partial waves. We emphasize that such an SU(3) symmetry breaking at NLO is well in line with χ EFT and the associated power counting [13, 44].

Analysis: The combined analysis of scattering and femtoscopic data is based on 12 data points for the *p* Λ elastic cross section, as well as six *p* Λ correlation functions measured in different ranges of pair transverse mass m_T in pp collisions at 13 TeV. In particular, six points of the cross section stem from the work of Alexander et al. [17], where we opt for those from the second choice of binning described in the corresponding work, while the remaining six data points are taken from the work of Sechi-Zorn et al. [16]. The femtoscopy data originates from the ALICE measurement of the *p* Λ correlation function in high-multiplicity (HM) pp collisions at 13 TeV [42]. When analyzed below the $N\Sigma$ threshold, the *S*-waves are sufficient to account for the interaction. The parameters of the repulsive core $V_C(r)$ in Eq. (1) are fitted independently for the spin singlet ($S=0$) and triplet ($S=1$) states, resulting in a total of 6 free parameters. The Usmani potential has been integrated into the CATS framework [45], which is capable of evaluating the corresponding cross section and correlation function by solving the Schrödinger equation. While this is sufficient to describe the cross section data, femtoscopic data necessitates additional knowledge of the two-particle emission source $S(m_T, r)$, as demanded by the Koonin-Pratt equation [46]

$$C(k) = \int S(m_T, r) \left| \Psi(\vec{k}, \vec{r}) \right|^2 d^3r. \quad (2)$$

Here, $C(k)$ represents the correlation as a function of the single-particle momentum k in the pair rest frame, while $\Psi(\vec{k}, \vec{r})$ is the wave function of the relative motion of the pair. The source $S(m_T, r)$ is provided as a function of the relative distance between the particles r at the moment of their effective emission. The modeling of the source in small collision systems at the LHC has been extensively studied in several recent works [42, 47, 48], which provide compatible results on the source properties. In the present analysis we adopt the CECA model [47], which operates based on a common emission source for all primordial particles, accounting for particle production through the decay of short-lived resonances and incorporating an intrinsic m_T scaling of the source size, as observed in the data. The CECA framework utilizes three fit parameters, for

details refer to [47]. For the ALICE data sample used in this work, the “standard candle” used to calibrate the source is the pp correlation, which has been measured differentially in m_T [42, 49]. In the present analysis, we perform a pre-fit of the pp correlations using the Argonne $v18$ potential [50], following the same procedure as described in [47]. However, out of the seven available m_T bins, we have omitted the last two due to issues with convergence at very low k . To eliminate any bias related to the assumption of a common source, the extracted source parameters from the pre-fit of the pp correlations are used as an initial guess for the pA system, after which they are re-fitted alongside the six interaction parameters, allowing a variation of 3 standard deviations (σ). Finally, we verify that the parameters converge to a proper local minimum without reaching the limiting values. The remaining details on both the pp and pA fits, such as the inclusion of momentum resolution, feed-down, non-femtoscopic baseline, etc., are mirrored from the analysis of the same data described in [47].

The first objective of the present analysis is to quantify the allowed scattering lengths in the spin singlet/triplet channels ($f_{0/1}$), which can be accomplished by considering potentials of varying strengths in the CATS framework. Note that we use the sign convention where attractive/repulsive interactions are characterized by positive/negative scattering lengths. Both the cross section and the correlation function are composed of a weighted sum of the two channels, with respective weights of 1/4 and 3/4. The two spin states are attractive and exhibit similar correlation shapes that differ in magnitude. Due to this similarity, the present analysis is not particularly sensitive to the individual scattering lengths of each spin channel, and a unique solution is not expected. Nevertheless, requiring that the two-body forces alone produce a bound hypertriton puts a lower limit on the strength of the interaction in the spin singlet channel. A concrete estimate is difficult to provide, however, judging from results for the hypertriton separation energy from Faddeev calculations employing modern YN potentials [14, 15], values of $f_0 \lesssim 2.0$ fm are not realistic. Assuming that the hypertriton is solely bound by three-body forces is likewise unrealistic given the present estimates [51] and explicit calculations [52] of their possible contribution. In view of this the scan is performed for $f_0 > 1.6$ fm. The lack of a unique solution leads to convergence issues in the fit procedure. To address this problem, multiple fits are performed, each constrained within a specific small region of f_0 and f_1 values. The procedure is repeated until the entire desired phase space is scanned. The best χ^2 of each individual step

is saved, allowing the creation of an exclusion plot for f_0 and f_1 . The estimator for the exclusion is the total $\chi^2 = \chi^2_{\text{scattering}} + \chi^2_{\text{femtoscropy}}$. The χ^2 is converted into a number of standard deviations ($n\sigma$) with respect to the best solution, accounting for a total of 9 degrees of freedom [53].

Results: The exclusion plot based on results with the Usmani potential is shown in Fig. 1. The axes correspond to the scattering lengths in the singlet f_0 and triplet f_1 channel, while the color code contains information on the compatibility with the data. The left panel is based on the analysis of only the cross section, while the right panel is the final result based on the combined analysis of femtoscopic and scattering data. The gray dashed lines mark the 1, 2 and 3σ exclusion regions. The black solid line, in the right panel, marks the border of a 3σ deviation with respect to the scattering data alone and is identical to the outer most dashed line from the left panel, while the shaded area depicts the region of even worse compatibility. As expected, there is a strong correlation between f_0 and f_1 , and the inclusion of femtoscopy data into the analysis leads to a significant decrease in uncertainties. Values of $f_0 > 3.34$ fm or $f_1 < 1.18$ fm are disfavored by the data. The lower (upper) bound of f_0 (f_1) cannot be constrained within the investigated phase space. Figure 1 contains two vertical bars depicting the values of the scattering parameters based on the NLO19 [14] and the next-to-next-to-leading order N²LO [15] potentials. The size of the markers represents the uncertainties related to the employed regulator (cutoff Λ) in the chiral NY potentials. Both of these values are located approximately in the middle of the phase space region allowed by the scattering data alone, which is not surprising, as the LECs of those potentials have, up to now, been fitted to that data. Nevertheless, the enhanced sensitivity of the combined analysis shows that the predicted scattering lengths are disfavored by as much as 4.8σ in the case of N²LO. The NLO19 interaction is overall better in line with the present analysis, nevertheless, a systematic deviation of ca. $1-3\sigma$ is observed, depending on the cutoff value. Indeed, the predictions by the potential with cutoff $\Lambda = 600$ MeV of $f_0 = 2.91$ fm and $f_1 = 1.41$ fm are in relatively good agreement, resulting in a deviation from the best solution of 1.1σ . On the other hand, a best fit of f_1 , keeping $f_0 = 2.91$ fm fixed, yields $f_1 = 1.32 \pm 0.08$ fm. Clearly, due to the strong correlation between the two parameters, changing the value of f_0 will influence the outcome for f_1 . For example, fixing $f_0 = 2.1$ fm implies the value $f_1 = 1.56 \pm 0.11$ fm. Table I provides multiple examples for scattering parameters and their

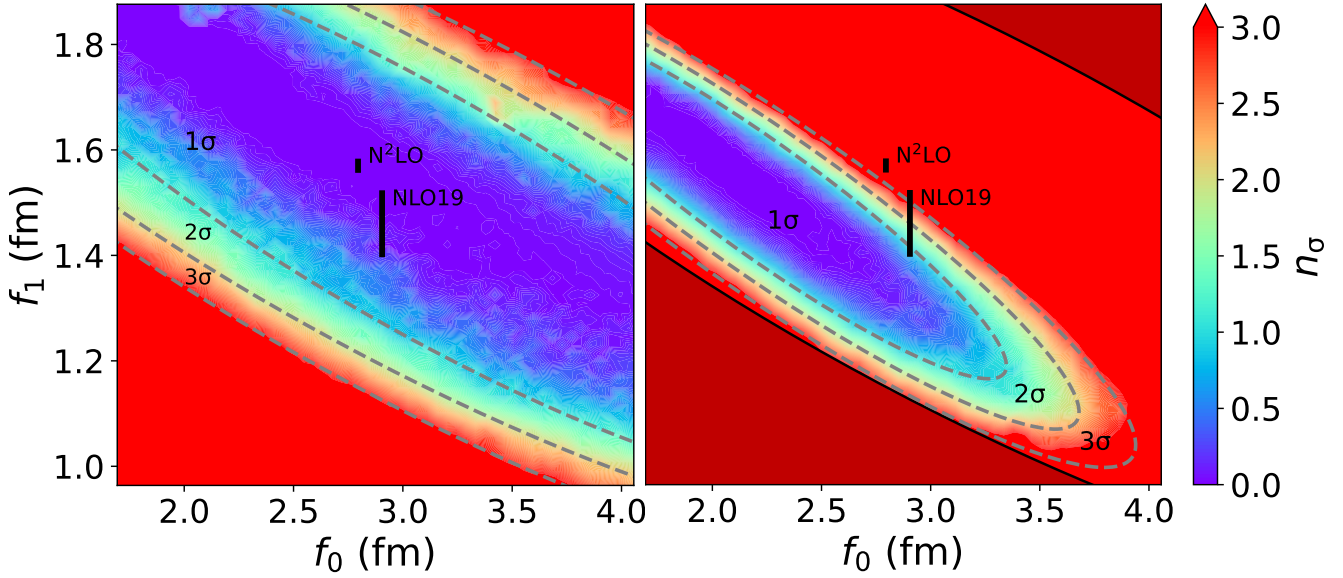


Figure 1. Exclusion plots for the singlet (f_0) and triplet (f_1) $p\Lambda$ scattering lengths based on the analysis of the cross section data (left panel) and on the combined analysis of cross section and correlation data (right panel). See text for details.

compatibility to the data. These results indicate an overall less attractive interaction compared to the published chiral potentials.

As a next step we explore how this less attractive Λ interaction affects predictions for the single-particle potential U_Λ at nuclear saturation density ρ_0 and its density dependence in general, considering the relevance of this quantity for the role of the Λ hyperon in neutron stars [9, 10]. In Fig. 2, we present results for the single-particle potential $U_\Lambda(k_\Lambda = 0)$ as a function of the nuclear matter density ρ , evaluated self-consistently within a conventional G -matrix calculation. We employ the formalism described in detail in Refs. [29, 54], where the so-called continuous choice is taken for the intermediate states, and the N^3 LO potential from [55] is used for the NN interaction. The NLO19(600) potential is chosen as starting point from which, by readjusting some of its LECs to reproduce 8 combinations of the Λ spin singlet and triplet scattering lengths within the 1σ region (points i to viii in Tab. I in the Appendix), we estimate the corresponding $U_\Lambda(\rho_0)$ given by the black square in Fig. 2. The vertical error bar represents the theoretical uncertainty estimated by considering the NLO19 potentials with different cutoffs (500 – 650 MeV), all refitted to describe the same set of scattering parameters. The final result is $U_\Lambda(\rho_0) = -36.3 \pm 1.3(\text{stat})_{-6.2}^{+2.5}(\text{syst})$ MeV, where the statistical uncertainty is associated with the data on the scattering parameters (right panel in Fig. 1) and the systematic with the cutoff dependence from the theory. The resulting theoretical uncertainty is large, as likewise reported in standard nuclear matter calculations

with chiral nucleon-nucleon potentials [56, 57]. Additionally, for the behavior of the potential depth as a function of ρ , we show in Fig. 2 the theoretical uncertainty (grey band) and the uncertainty from the combined data (yellow band). The predicted values for $U_\Lambda(\rho)$ are similar to

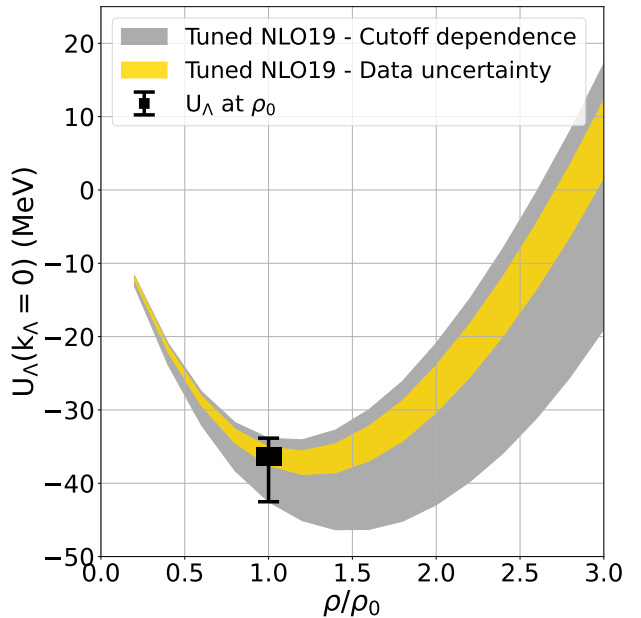


Figure 2. A single-particle potential U_Λ as a function of the nuclear-matter density ρ with $\rho_0 = 0.166 \text{ fm}^{-3}$ being the nuclear-matter saturation density.

the result for the original NLO19 potential. Our results

at ρ_0 lie below the usually cited semi-empirical value of $U_\Lambda = -28 \sim -30$ MeV obtained from hypernuclei constraints [1]. This is in line with comparable G -matrix calculations where a similar overbinding feature has been observed when two-body-only contributions are taken into account, as seen in, for example, [14, 58]. In two recent works [29, 30] an overall repulsion from a chiral NNY three-body force has been incorporated in the form of an effective density-dependent NY two-body potential [59]. This addition allows the authors to satisfy the ≈ -30 MeV hypernuclear constraint and, at the same time, suppresses the appearance of Λ hyperons for densities as realized in NS, i.e. offers a solution to the so-called ‘‘hyperon-puzzle’’ [2, 9]. Our results are compatible with such a strategy. Quantitative constraints on this effective three-body force might become available in future correlation studies [60, 61].

In conclusion, in this work we have presented the first combined analysis of low-energy femtoscopic and scattering data to constrain the S -wave scattering parameters of the $p\Lambda$ interaction, resulting in the tightest limits available for future theoretical studies. The $p\Lambda$ interaction is found to be overall less attractive than what has been indicated by the scattering data from the 1960s. We observe a strong, approximately linear, correlation between the values of the scattering lengths in the spin singlet and triplet states. The best solution, if f_0 is fixed to 2.1 fm, is $f_1 = 1.56 \pm 0.08$ fm. Lower f_0 values will eventually prohibit a hypertriton bound by two-body forces. The maximum (minimum) allowed values for f_0 (f_1) are 3.34 (1.18) fm.

Clearly, the accurate reproduction of low-energy NA data is an important requirement for realistic predictions of many-body systems. Thus, we have fine-tuned the chiral YN potential NLO19 to match the established scattering parameters in order to explore the impact on the in-medium properties of the Λ hyperon. The result with those NLO19 variants for $U_\Lambda(\rho_0)$ is ~ -36 MeV, which implies an overbinding with regard to the nominal Λ binding energy in infinite nuclear matter. This is consistent with the current notion of an additional repulsion acting on the Λ within the medium, attributed to many-body effects. The presented results can serve as a state-of-the-art guideline for the contribution to be expected from two-body $p\Lambda$ interactions.

We would like to thank Prof. L. Fabbietti for her support and fruitful discussions which helped us in finalizing these results. This work was supported by the ORIGINS cluster DFG under Germany’s Excellence Strategy - EXC2094 - 390783311 and the DFG through Grant SFB 1258 ‘‘Neutrinos and Dark Matter in Astro and Particle Physics’’. V. M. S. is supported by the Deutsche Forschungsgemeinschaft (DFG) through the

grant MA 8660/1 – 1.

APPENDIX

Table I presents several examples illustrating the compatibility of different scattering parameters with the data. The compatibility is estimated using the number of standard deviations, denoted as $n\sigma$, with respect to the best possible fit. We consider three scenarios: firstly, only the femtосcopy data is taken into account, resulting in $n\sigma_{\text{fmt}}$; secondly, only the scattering data is considered ($n\sigma_{\text{sct}}$); and thirdly, $n\sigma_{\text{tot}}$ corresponds to the combined analysis presented in this work. It is essential to note that these three scenarios represent independent analyses, each having a different best solution as a baseline. Consequently, there is no straightforward relation between the three estimators.

Table I. Summary table showing the compatibility of different scattering parameters to the femtосcopy data ($n\sigma_{\text{fmt}}$), scattering data ($n\sigma_{\text{sct}}$) as well as the combined analysis from the present work ($n\sigma_{\text{tot}}$).

Usmani parameterization	f_0 (fm)	f_1 (fm)	$n\sigma_{\text{fmt}}$	$n\sigma_{\text{sct}}$	$n\sigma_{\text{tot}}$
NLO13(600)	2.91	1.54	5.2	0.0	4.6
NLO19(600)	2.91	1.41	1.7	0.4	1.1
N ² LO(550)	2.79	1.58	5.4	0.0	4.8
i	2.10	1.44	0.2	2.1	1.0
ii	2.10	1.56	0.0	0.9	0.0
iii	2.10	1.66	1.8	0.2	1.0
iv	2.50	1.54	1.7	0.2	1.0
v	2.50	1.46	0.2	0.8	0.0
vi	2.50	1.55	1.8	0.2	1.0
vii	2.91	1.32	0.1	1.5	0.3
viii	3.34	1.18	1.2	0.9	1.0

* dimitar.mihaylov@mytum.de

† j.haidenbauer@fz-juelich.de

‡ valentina.mantovani-sarti@tum.de

- [1] A. Gal, E. V. Hungerford, and D. J. Millener. Strangeness in nuclear physics. *Rev. Mod. Phys.*, 88(3):035004, 2016. [arXiv:1605.00557](#), [doi:10.1103/RevModPhys.88.035004](#).
- [2] Laura Tolos and Laura Fabbietti. Strangeness in Nuclei and Neutron Stars. *Prog. Part. Nucl. Phys.*, 112:103770, 2020. [arXiv:2002.09223](#), [doi:10.1016/j.ppnp.2020.103770](#).

- [3] B. P. Abbott et al. GW170817: Observation of Gravitational Waves from a Binary Neutron Star Inspiral. *Phys. Rev. Lett.*, 119(16):161101, 2017. [arXiv:1710.05832](#), [doi:10.1103/PhysRevLett.119.161101](#).
- [4] B. P. Abbott et al. Multi-messenger Observations of a Binary Neutron Star Merger. *Astrophys. J. Lett.*, 848(2):L12, 2017. [arXiv:1710.05833](#), [doi:10.3847/2041-8213/aa91c9](#).
- [5] M. C. Miller et al. PSR J0030+0451 Mass and Radius from *NICER* Data and Implications for the Properties of Neutron Star Matter. *Astrophys. J. Lett.*, 887(1):L24, 2019. [arXiv:1912.05705](#), [doi:10.3847/2041-8213/ab50c5](#).
- [6] M. C. Miller et al. The Radius of PSR J0740+6620 from *NICER* and XMM-Newton Data. *Astrophys. J. Lett.*, 918(2):L28, 2021. [arXiv:2105.06979](#), [doi:10.3847/2041-8213/ac089b](#).
- [7] Thomas E. Riley et al. A *NICER* View of PSR J0030+0451: Millisecond Pulsar Parameter Estimation. *Astrophys. J. Lett.*, 887(1):L21, 2019. [arXiv:1912.05702](#), [doi:10.3847/2041-8213/ab481c](#).
- [8] Thomas E. Riley et al. A *NICER* View of the Massive Pulsar PSR J0740+6620 Informed by Radio Timing and XMM-Newton Spectroscopy. *Astrophys. J. Lett.*, 918(2):L27, 2021. [arXiv:2105.06980](#), [doi:10.3847/2041-8213/ac0a81](#).
- [9] Debarati Chatterjee and Isaac Vidaña. Do hyperons exist in the interior of neutron stars? *Eur. Phys. J. A*, 52(2):29, 2016. [arXiv:1510.06306](#), [doi:10.1140/epja/i2016-16029-x](#).
- [10] Jürgen Schaffner-Bielich. *Compact Star Physics*. Cambridge University Press, 8 2020. [doi:10.1017/9781316848357](#).
- [11] B. Povh. Nuclear Physics With Hyperons. *Prog. Part. Nucl. Phys.*, 5:245–268, 1981. [doi:10.1016/0146-6410\(81\)90051-x](#).
- [12] Steven Weinberg. Nuclear forces from chiral Lagrangians. *Phys. Lett. B*, 251:288–292, 1990. [doi:10.1016/0370-2693\(90\)90938-3](#).
- [13] J. Haidenbauer, S. Petschauer, N. Kaiser, U.-G. Meißner, A. Nogga, and W. Weise. Hyperon-nucleon interaction at next-to-leading order in chiral effective field theory. *Nucl. Phys. A*, 915:24–58, 2013. [arXiv:1304.5339](#), [doi:10.1016/j.nuclphysa.2013.06.008](#).
- [14] J. Haidenbauer, U.-G. Meißner, and A. Nogga. Hyperon-nucleon interaction within chiral effective field theory revisited. *Eur. Phys. J. A*, 56(3):91, 2020. [arXiv:1906.11681](#), [doi:10.1140/epja/s10050-020-00100-4](#).
- [15] Johann Haidenbauer, Ulf-G. Meißner, Andreas Nogga, and Hoai Le. Hyperon-nucleon interaction in chiral effective field theory at next-to-next-to-leading order. *Eur. Phys. J. A*, 59(3):63, 2023. [arXiv:2301.00722](#), [doi:10.1140/epja/s10050-023-00960-6](#).
- [16] B. Sechi-Zorn, B. Kehoe, J. Twitty, and R. A. Burnstein. Low-Energy Λ -Proton Elastic Scattering. *Phys. Rev.*, 175:1735–1740, 1968. [doi:10.1103/PhysRev.175.1735](#).
- [17] G. Alexander, U. Karshon, A. Shapira, G. Yekutieli, R. Engelmann, H. Filthuth, and W. Lughofer. Study of the Λ -N system in low-energy Λ -p elastic scattering. *Phys. Rev.*, 173:1452–1460, 1968. [doi:10.1103/PhysRev.173.1452](#).
- [18] F. Eisele, H. Filthuth, W. Foehlich, V. Hepp, and Gunter Zech. Elastic Σ^+ -p scattering at low energies. *Phys. Lett. B*, 37:204–206, 1971. [doi:10.1016/0370-2693\(71\)90053-0](#).
- [19] O. Hashimoto and H. Tamura. Spectroscopy of Lambda hypernuclei. *Prog. Part. Nucl. Phys.*, 57:564–653, 2006. [doi:10.1016/j.pnpnp.2005.07.001](#).
- [20] M. Röder et al. Final-State Interactions in the Process $\bar{p}p \rightarrow pK^+\Lambda$. *Eur. Phys. J. A*, 49:157, 2013. [arXiv:1305.0451](#), [doi:10.1140/epja/i2013-13157-9](#).
- [21] F. Hauenstein et al. Determination of the spin triplet $p\Lambda$ scattering length from the final state interaction in the $\bar{p}p \rightarrow pK^+\Lambda$ reaction. *Phys. Rev. C*, 95(3):034001, 2017. [arXiv:1607.04783](#), [doi:10.1103/PhysRevC.95.034001](#).
- [22] J. Rowley et al. Improved Λp Elastic Scattering Cross Sections Between 0.9 and 2.0 GeV/c and Connections to the Neutron Star Equation of State. *Phys. Rev. Lett.*, 127(27):272303, 2021. [arXiv:2108.03134](#), [doi:10.1103/PhysRevLett.127.272303](#).
- [23] K. Miwa et al. Precise measurement of differential cross sections of the $\Sigma^-p \rightarrow \Lambda n$ reaction in momentum range 470–650 MeV/c. *Phys. Rev. Lett.*, 128(7):072501, 2022. [arXiv:2111.14277](#), [doi:10.1103/PhysRevLett.128.072501](#).
- [24] K. Miwa et al. Measurement of the differential cross sections of the Σ^-p elastic scattering in momentum range 470 to 850 MeV/c. *Phys. Rev. C*, 104(4):045204, 2021. [arXiv:2104.13608](#), [doi:10.1103/PhysRevC.104.045204](#).
- [25] T. Nanamura et al. Measurement of differential cross sections for $\Sigma+p$ elastic scattering in the momentum range 0.44–0.80 GeV/c. *PTEP*, 2022(9):093D01, 2022. [arXiv:2203.08393](#), [doi:10.1093/ptep/ptac101](#).
- [26] Shreyasi Acharya et al. ${}^3_\Lambda\text{H}$ and ${}^3_\Lambda\bar{\text{H}}$ lifetime measurement in Pb-Pb collisions at $\sqrt{s_{\text{NN}}} = 5.02$ TeV via two-body decay. *Phys. Lett. B*, 797:134905, 2019. [arXiv:1907.06906](#), [doi:10.1016/j.physletb.2019.134905](#).
- [27] J. Adam et al. Measurement of the mass difference and the binding energy of the hypertriton and antihypertriton. *Nature Phys.*, 16(4):409–412, 2020. [arXiv:1904.10520](#), [doi:10.1038/s41567-020-0799-7](#).
- [28] D. J. Millener, C. B. Dover, and A. Gal. Lambda Nucleus Single Particle Potentials. *Phys. Rev. C*, 38:2700–2708, 1988. [doi:10.1103/PhysRevC.38.2700](#).
- [29] Dominik Gerstung, Norbert Kaiser, and Wolfram Weise. Hyperon-nucleon three-body forces and strangeness in neutron stars. *Eur. Phys. J. A*, 56:175, 2020. [arXiv:2001.10563](#), [doi:10.1140/epja/s10050-020-00180-2](#).
- [30] Domenico Logoteta, Isaac Vidaña, and Ignazio Bombaci. Impact of chiral hyperonic three-body forces on neutron stars. *Eur. Phys. J. A*, 55(11):207, 2019. [arXiv:1906.11722](#), [doi:10.1140/epja/i2019-12909-9](#).
- [31] L. Fabbietti, V. Mantovani Sarti, and O. Vazquez Doce. Study of the Strong Interaction Among Hadrons with Correlations at the LHC. *Ann. Rev. Nucl. Part. Sci.*, 71:377–402, 2021. [arXiv:2012.09806](#), [doi:10.1146/annurev-nucl-102419-034438](#).
- [32] Shreyasi Acharya et al. Exploring the $\text{NA}-\text{N}\Sigma$ coupled system with high precision correlation techniques at the LHC. *Phys. Lett. B*, 833:137272, 2022. [arXiv:](#)

- 2104.04427, doi:10.1016/j.physletb.2022.137272.
- [33] Shreyasi Acharya et al. Investigation of the p - Σ 0 interaction via femtoscopy in pp collisions. *Phys. Lett. B*, 805:135419, 2020. arXiv:1910.14407, doi:10.1016/j.physletb.2020.135419.
- [34] Shreyasi Acharya et al. First Observation of an Attractive Interaction between a Proton and a Cascade Baryon. *Phys. Rev. Lett.*, 123(11):112002, 2019. arXiv:1904.12198, doi:10.1103/PhysRevLett.123.112002.
- [35] Alice Collaboration et al. Unveiling the strong interaction among hadrons at the LHC. *Nature*, 588:232–238, 2020. [Erratum: *Nature* 590, E13 (2021)]. arXiv:2005.11495, doi:10.1038/s41586-020-3001-6.
- [36] Shreyasi Acharya et al. First measurement of the Λ - Ξ interaction in proton–proton collisions at the LHC. *Phys. Lett. B*, 844:137223, 2023. arXiv:2204.10258, doi:10.1016/j.physletb.2022.137223.
- [37] J. Adamczewski-Musch et al. The Λp interaction studied via femtoscopy in $p + \text{Nb}$ reactions at $\sqrt{s_{\text{NN}}} = 3.18 \text{ GeV}$. *Phys. Rev. C*, 94(2):025201, 2016. arXiv:1602.08880, doi:10.1103/PhysRevC.94.025201.
- [38] Kazuya Aoki et al. Extension of the J-PARC Hadron Experimental Facility: Third White Paper. 10 2021. arXiv:2110.04462.
- [39] Future high-energy pp programme with ALICE. 2020.
- [40] A. R. Bodmer, Q. N. Usmani, and J. Carlson. Binding energies of hypernuclei and three-body LNN forces. *Phys. Rev. C*, 29:684–687, 1984. doi:10.1103/PhysRevC.29.684.
- [41] Fu-Qiang Wang and Scott Pratt. Lambda proton correlations in relativistic heavy ion collisions. *Phys. Rev. Lett.*, 83:3138–3141, 1999. arXiv:nucl-th/9907019, doi:10.1103/PhysRevLett.83.3138.
- [42] Shreyasi Acharya et al. Search for a common baryon source in high-multiplicity pp collisions at the LHC. *Phys. Lett. B*, 811:135849, 2020. arXiv:2004.08018, doi:10.1016/j.physletb.2020.135849.
- [43] Hoai Le, Johann Haidenbauer, Ulf-G. Meißner, and Andreas Nogga. Implications of an increased Λ -separation energy of the hypertriton. *Phys. Lett. B*, 801:135189, 2020. arXiv:1909.02882, doi:10.1016/j.physletb.2019.135189.
- [44] Stefan Petschauer and Norbert Kaiser. Relativistic SU(3) chiral baryon–baryon Lagrangian up to order q^2 . *Nucl. Phys. A*, 916:1–29, 2013. arXiv:1305.3427, doi:10.1016/j.nuclphysa.2013.07.010.
- [45] D. L. Mihaylov, V. Mantovani Sarti, O. W. Arnold, L. Fabbietti, B. Hohlweger, and A. M. Mathis. A femtosopic Correlation Analysis Tool using the Schrödinger equation (CATS). *Eur. Phys. J. C*, 78(5):394, 2018. arXiv:1802.08481, doi:10.1140/epjc/s10052-018-5859-0.
- [46] Michael Annan Lisa, Scott Pratt, Ron Soltz, and Urs Wiedemann. Femtoscopy in relativistic heavy ion collisions. *Ann. Rev. Nucl. Part. Sci.*, 55:357–402, 2005. arXiv:nucl-ex/0505014, doi:10.1146/annurev.nucl.55.090704.151533.
- [47] Dimitar Mihaylov and Jaime González González. Novel model for particle emission in small collision systems. *Eur. Phys. J. C*, 83(7):590, 2023. arXiv:2305.08441, doi:10.1140/epjc/s10052-023-11774-7.
- [48] Shreyasi Acharya et al. Common femtosopic hadron-emission source in pp collisions at the LHC. 11 2023. arXiv:2311.14527.
- [49] ALICE Collaboration. Supplemental figures: “Search for a common baryon source in high-multiplicity pp collisions at the LHC”. CERN-EP-2020-053, 2023.
- [50] Robert B. Wiringa, V. G. J. Stoks, and R. Schiavilla. An Accurate nucleon–nucleon potential with charge independence breaking. *Phys. Rev. C*, 51:38–51, 1995. arXiv:nucl-th/9408016, doi:10.1103/PhysRevC.51.38.
- [51] Hoai Le, Johann Haidenbauer, Ulf-G. Meißner, and Andreas Nogga. Separation energies of light Λ hypernuclei and their theoretical uncertainties. 8 2023. arXiv:2308.01756.
- [52] M. Kohno, H. Kamada, and K. Miyagawa. Contributions of 2π -exchange, 1π -exchange, and contact three-body forces in NNLO ChEFT to ${}^3_\Lambda\text{H}$. 11 2023. arXiv:2311.10923.
- [53] William H. Press, Saul A. Teukolsky, William T. Vetterling, and Brian P. Flannery. *Numerical Recipes 3rd Edition: The Art of Scientific Computing*, chapter 15.6. Cambridge University Press, New York, NY, USA, 3 edition, 2007.
- [54] S. Petschauer, J. Haidenbauer, N. Kaiser, Ulf-G. Meißner, and W. Weise. Hyperons in nuclear matter from SU(3) chiral effective field theory. *Eur. Phys. J. A*, 52(1):15, 2016. arXiv:1507.08808, doi:10.1140/epja/i2016-16015-4.
- [55] D. R. Entem and R. Machleidt. Accurate charge dependent nucleon nucleon potential at fourth order of chiral perturbation theory. *Phys. Rev. C*, 68:041001, 2003. arXiv:nucl-th/0304018, doi:10.1103/PhysRevC.68.041001.
- [56] F. Sammarruca, L. Coraggio, J. W. Holt, N. Itaco, R. Machleidt, and L. E. Marcucci. Toward order-by-order calculations of the nuclear and neutron matter equations of state in chiral effective field theory. *Phys. Rev. C*, 91(5):054311, 2015. arXiv:1411.0136, doi:10.1103/PhysRevC.91.054311.
- [57] Jinniu Hu, Ying Zhang, Evgeny Epelbaum, Ulf-G Meißner, and Jie Meng. Nuclear matter properties with nucleon–nucleon forces up to fifth order in the chiral expansion. *Phys. Rev. C*, 96(3):034307, 2017. arXiv:1612.05433, doi:10.1103/PhysRevC.96.034307.
- [58] T. A. Rijken, V. G. J. Stoks, and Y. Yamamoto. Soft core hyperon - nucleon potentials. *Phys. Rev. C*, 59:21–40, 1999. arXiv:nucl-th/9807082, doi:10.1103/PhysRevC.59.21.
- [59] Stefan Petschauer, Johann Haidenbauer, Norbert Kaiser, Ulf-G. Meißner, and Wolfram Weise. Density-dependent effective baryon–baryon interaction from chiral three-baryon forces. *Nucl. Phys. A*, 957:347–378, 2017. arXiv:1607.04307, doi:10.1016/j.nuclphysa.2016.09.010.
- [60] A. Kievsky, E. Garrido, M. Viviani, L. E. Marcucci, L. Serksnyte, and R. Del Grande. The nnn and ppp correlation functions. 10 2023. arXiv:2310.10428.
- [61] Shreyasi Acharya et al. Towards the understanding of the genuine three-body interaction for p - p - p and p - p - Λ . *Eur. Phys. J. A*, 59(7):145, 2023. arXiv:2206.03344, doi:10.1140/epja/s10050-023-00998-6.